Academic Journal of Science and Technology
ISSN: 2771-3032 | Vol. 20, No. 1, 2026

qBIC-Enhanced True Chiral Nonlinear Response in a Monolayer WS_2 Hybrid Metasurface

Gaojing Liu and Ziming Meng

School of Physics and Optoelectronic Engineering, Guangdong University of Technology, Guangzhou, Guangdong, 510000, China

Abstract: Hybrid dielectric metasurfaces that combine true chirality, quasi-bound states in the continuum (qBICs), and the strong second-order nonlinearity of two-dimensional semiconductors provide an efficient route toward chirality-selective nonlinear optics. Based on the supplied simulation results, this paper presents a systematic analysis of a truly chiral G-shaped metasurface composed of TiO_2, SiO_2, and WS_2. The structure breaks symmetry through its planar G-shaped geometry, vertical layered stacking, and a 10° perturbation, thereby transforming an originally symmetry-protected bound state in the continuum into an externally excitable qBIC mode. As a result, a high-Q resonance, pronounced circular dichroism, and strong near-field localization emerge around 794.7 nm. The circularly polarized transmission spectra indicate strong spin-selective coupling, while the magnetic-field maps further reveal markedly different hotspot patterns near the active interface under opposite helicities. When combined with the second-order polarization response of WS_2, the device exhibits an approximately 29.2-fold helicity contrast in nonlinear frequency conversion. The physical mechanisms reflected in each figure are further clarified from the perspectives of multipolar interference, coupled-mode physics, and field-material overlap. Taken together, the dataset forms a coherent scientific narrative: geometric symmetry breaking opens the qBIC channel, true chirality endows the resonance with helicity selectivity, and the localized resonant field enhances the second-order nonlinearity of WS_2, ultimately enabling highly selective nonlinear conversion.

Keywords: True Chirality; Bound States in the Continuum; Dielectric Metasurfaces; WS_2; Nonlinear Frequency Conversion; Circular Dichroism.

1. Introduction

Chiral light-matter interaction is a central theme in nanophotonics because it unifies polarization, symmetry, and device functionality within a common physical framework. Chiral photonic structures respond differently to left- and right-circularly polarized light, and this difference can manifest not only in propagation, absorption, and scattering, but also in field-enhanced nonlinear processes [5,6]. With the rapid development of two-dimensional materials, subwavelength resonators, and metasurfaces, an important current objective is to construct strong chiral responses on the micro- and nanoscale and convert them efficiently into measurable nonlinear outputs.

At the same time, bound states in the continuum (BICs) and quasi-bound states in the continuum (qBICs) have become key concepts in resonant nanophotonics [1-4]. An ideal BIC is an eigenstate embedded in the radiation continuum that does not radiate outward and therefore possesses, in theory, an infinite quality factor. When a weak perturbation breaks the original symmetry of the structure, however, the mode can couple to free space in the form of a qBIC while still preserving a high Q factor and strong field confinement. Such modes are particularly attractive for enhancing nonlinear optical effects because nonlinear signals are extremely sensitive to the local electromagnetic field intensity.

Among the most promising strategies is to combine chirality with qBIC physics [6-8]. If the geometric perturbation that opens the BIC channel simultaneously breaks the mirror symmetry relevant to circular polarization, the resonance can couple to opposite helicities with markedly different strengths, thereby producing strong circular dichroism, helicity-selective transmission, and helicity-dependent near-field enhancement. This mechanism is important not only for linear polarization control, but also for chirality-selective nonlinear emission, frequency conversion, and polarization-sensitive detection.

Monolayer transition-metal dichalcogenides (TMDs), such as WS_2 and MoS_2, are ideal nonlinear media for this purpose [9-12]. Because they intrinsically lack inversion symmetry, these materials exhibit strong second-order nonlinear responses and can support efficient second-harmonic generation and related frequency-conversion processes even at atomic-layer thickness. However, the interaction length between a freestanding two-dimensional material and free-space light is inherently limited. High-Q resonant structures are therefore required to increase the local field intensity and the light-matter overlap so that the intrinsic nonlinear potential of the material can be fully released [13-15].

The supplied figures describe precisely such a hybrid platform: a G-shaped $TiO_2/SiO_2/WS_2$ metasurface that exhibits true chirality, a narrowband spectral response near 794.7 nm, pronounced circular dichroism, and a large nonlinear conversion contrast. The purpose of this paper is not merely to describe the figures one by one, but to organize them into a complete physical chain: how the structure breaks symmetry, how the qBIC is excited, how the linear chiral response is formed, how the near-field hotspots are established, and how the nonlinearity of WS_2 is selectively enhanced by the resonant field. Guided by this narrative, the following sections examine the result, significance, and mechanism represented by each figure in detail.

2. Device Architecture and Physical Picture

Figure 1 establishes the structural foundation of the entire device. The unit cell of the metasurface consists of a G-shaped

TiO_2 resonator, a SiO_2 supporting layer, and a WS_2 nonlinear layer placed close to the resonantly active region. The figure specifies the key geometric parameters, including the lattice constant p, the arm length and width of the G-shaped element, the height, and the interlayer thicknesses. Together, these parameters determine the mode volume, radiation leakage, near-field distribution, and operating wavelength. Compared with conventional symmetric disks or square pillars, the G-shaped unit possesses a stronger geometric bias and is therefore more favorable for supporting intrinsic chiral responses associated with coupling to circularly polarized light.

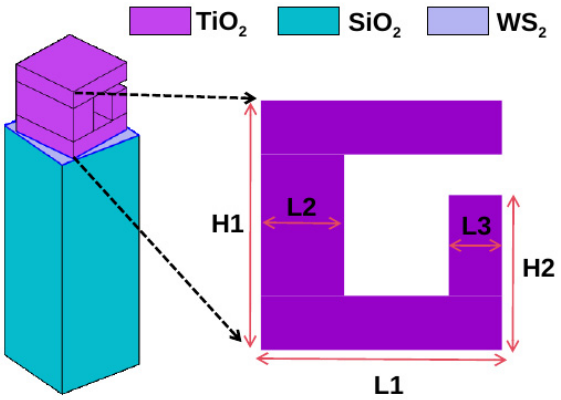


Figure 1. Geometric structure of the truly chiral hybrid metasurface composed of TiO_2, SiO_2, and WS_2. The G-shaped resonator introduces in-plane asymmetry, while layered stacking and a 10° perturbation provide out-of-plane coupling and the opening condition for the Qbic

This geometry is meaningful from both resonant and symmetry-related perspectives. In an ideal high-symmetry configuration, a dielectric metasurface can support a symmetry-protected BIC mode that does not couple to the free-space radiation channel [1,2]. Once the G-shaped geometry is introduced and a further 10° perturbation is applied, the original symmetry is partially broken and the ideal BIC is converted into an externally excitable qBIC. In other words, the mode is no longer completely dark, but instead appears as a narrow spectral feature in transmission or scattering while retaining the two key advantages of a high Q factor and strong field localization.

The same structure also naturally exhibits true chirality. The G-shaped contour strongly breaks the in-plane mirror symmetry, while the vertical $TiO_2/WS_2/SiO_2$ layered stacking introduces out-of-plane asymmetry [6-8]. Only when both in-plane and out-of-plane asymmetries coexist does the system acquire genuine three-dimensional chirality rather than an apparent chirality defined only by the incidence or observation direction. For this reason, the coupling probabilities for left- and right-circularly polarized light become strongly split.

A representative qBIC scaling law can be written as

$$Q_{\mathrm{rad}} \propto 1/\delta^2 \qquad (1)$$

where δ denotes the effective symmetry-breaking parameter associated with the 10° perturbation. Equation (1) reflects the characteristic trade-off of qBIC physics: a smaller perturbation yields a higher Q factor but weaker external coupling, whereas a larger perturbation increases radiation leakage and improves excitability at the cost of broader linewidth. The present structure therefore operates near a balance point between accessibility and strong field enhancement [2,3].

Because the active material is WS_2, the nonlinear process can naturally be understood as a second-order frequency-conversion process. The nonlinear polarization can be expressed as

$$P_i(2\omega) = \varepsilon_0 \Sigma_{jk} \chi_{ijk}^{(2)} E_j(\omega) E_k(\omega) \qquad (2)$$

This expression already reveals the basic design logic of the device: the output signal depends both on the intrinsic second-order susceptibility tensor of WS_2 and on the pump-field intensity established locally by the qBIC mode. If one incident helicity excites a stronger local field than the other, it will induce a stronger second-order polarization inside WS_2 and will eventually produce a pronounced chiral contrast in the nonlinear output [10-13].

3. Linear Chiral Response of the qBIC Resonance

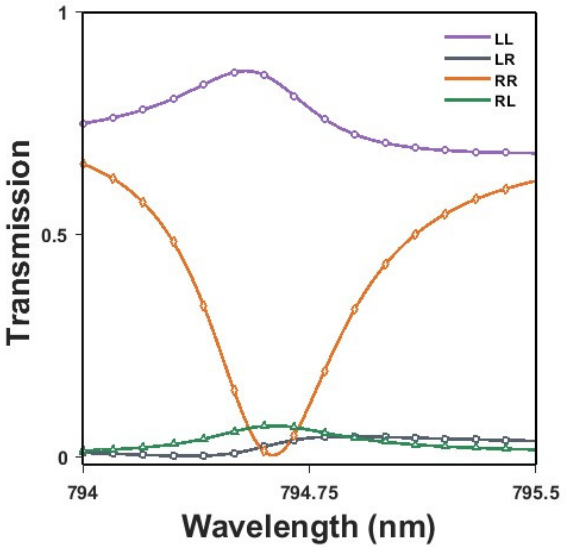


Figure 2. Circularly polarized transmission spectra of the metasurface. At the resonance, the transmission coefficients are LL = 0.87, LR = 0.02, RR ≈ 0, and RL = 0.06, indicating strong helicity-selective coupling

Figures 2 and 3 together summarize the linear chiral response of the device. Figure 2 presents the transmission coefficients in the circular-polarization basis: LL, LR, RR, and RL. Near the resonance around 794.7-794.8 nm, the values indicated in the figure are LL = 0.87, LR = 0.02, RR ≈ 0, and RL = 0.06. Here, the two subscripts denote the incident and transmitted circular polarizations, respectively. These results therefore reveal not only the total transmission strength but also the competition between co-polarized and cross-polarized channels.

Two important conclusions follow immediately. First, the resonance can be efficiently excited by only one circularly polarized helicity, whereas the opposite helicity is strongly suppressed. Second, the cross-polarized channels remain relatively weak, indicating that the dominant physical process is not a simple polarization flip, but rather chirality-selective resonant coupling. In other words, true chirality and qBIC physics are not independent features in this structure; instead, they jointly determine both the shape and strength of the

spectral response.

Figure 3 conveys the same physical process in a more compact form, namely through the circular-dichroism (CD) spectrum. A commonly used transmission-based definition is

$$\mathrm{CD} = (T_L - T_R)/(T_L + T_R) \quad (3)$$

The peak value reaches 0.94 in the supplied plot, which is remarkably high for a dielectric metasurface operating within such a narrow spectral window. Physically, a CD value approaching 1 means that one helicity couples efficiently to the resonant mode while the opposite helicity is almost excluded. Because the two circular polarizations would be equivalent in an ideal achiral structure, such a high CD directly proves that the device supports a strong and intrinsic true-chiral response [5-8].

The complementary behavior of the curves in Figure 2 is itself a hallmark of a chiral qBIC. The favored helicity channel exhibits a strong and clearly resolved resonant signature, whereas the disfavored co-polarized channel remains nearly dark. The cross-polarized terms are not exactly zero, but they are much smaller than the dominant channel. This indicates that the chiral coupling in the structure is governed neither by pure mode conversion nor by a simple absorption difference, but by the combined action of chirality-selective mode excitation and radiation interference.

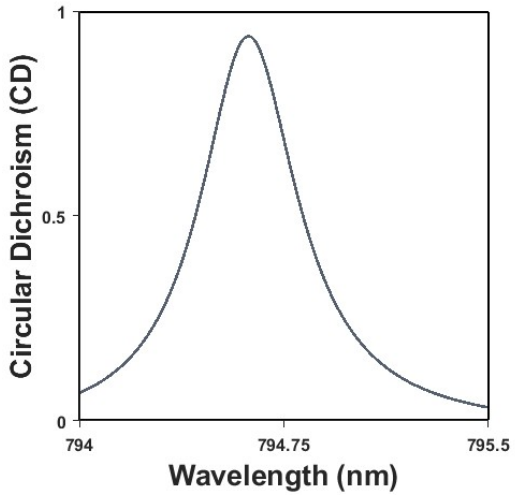


Figure 3. Circular-dichroism spectrum of the device. Near the qBIC resonance, the CD peak reaches 0.94, confirming strong discrimination between opposite helicities.

4. Helicity-Selective Near-Field Distribution and qBIC Mechanism

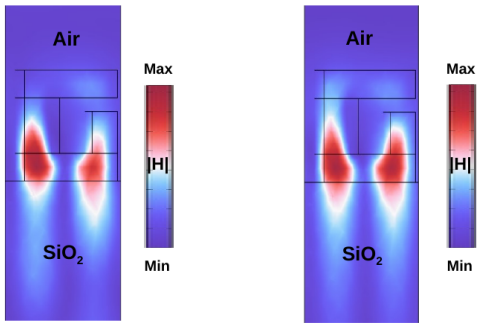


Figure 4. Magnetic-field intensity |H| distributions under LCP (left) and RCP (right) excitation. The different hotspot patterns show that the resonant build-up near the active interface depends strongly on the incident helicity.

Figure 4 provides the missing link between the linear chiral response and the nonlinear enhancement. It shows the magnetic-field intensity |H| distributions under LCP and RCP excitation. The field maps are clearly different for the two cases: one helicity produces stronger and more concentrated hotspots inside the G-shaped cavity and near the interface, whereas the other leads to a weaker and more diffuse field pattern. This demonstrates that circular polarization affects not only far-field transmission but also the local energy storage and effective mode volume.

This behavior can be understood from the viewpoint of multipolar interference. In dielectric metasurfaces, a qBIC may be regarded as a high-Q mode that emerges when several radiating multipolar contributions nearly cancel one another in the far field [1-3]. When the structure is truly chiral, opposite helicities do not excite these multipolar components with identical phases and amplitudes. As a result, one helicity approaches the condition of radiation cancellation and field trapping more closely, whereas the other deviates from it. Therefore, even though the two excitations differ only by their handedness, the internal field distributions established within the resonance can become dramatically different [7,8].

Figure 4 is a direct visualization of this mechanism. The field pattern associated with one helicity is better matched to the gaps and asymmetric arm segments of the G-shaped cavity, so energy can be injected into the qBIC mode more efficiently. The opposite helicity, by contrast, suffers from less favorable phase matching and symmetry-selection rules, making it difficult to form equally strong hotspots at the same locations. The linear circular dichroism of the device is thus converted, at the near-field level, into hotspot selectivity.

This field map also highlights the importance of the vertical stack. The labels 'Air' and 'SiO_2' show that the strongest hotspots are located close to the interface region, which is precisely where a two-dimensional material should be placed. Because WS_2 is only atomically thin, the material can truly benefit from qBIC-enhanced fields only when the hotspots fall in its immediate vicinity. The out-of-plane layered design is therefore not an auxiliary detail, but a key requirement for achieving strong overlap between the near field and the two-dimensional nonlinear medium [13-15].

5. Enhanced Nonlinear Frequency Conversion in the WS_2 Layer

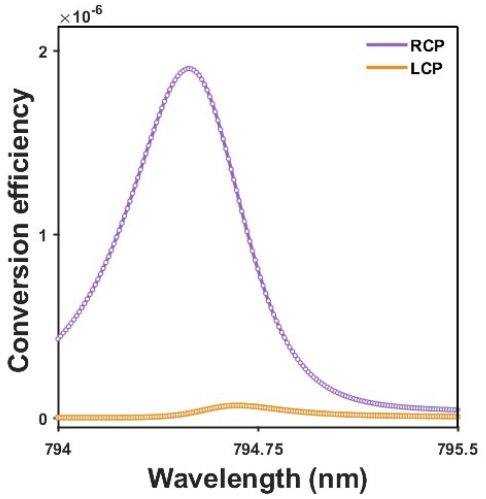


Figure 5. Nonlinear conversion efficiency under circularly polarized excitation. The peak conversion efficiency is 1.9 × 10^-6 under RCP excitation and 6.5 × 10^-8 under LCP excitation, corresponding to a contrast of approximately 29.2.

Figure 5 presents the nonlinear conversion efficiency under circularly polarized excitation, and this is the central result of the study. Under RCP excitation, the peak conversion efficiency reaches 1.9 × 10^-6, whereas under LCP excitation it is only 6.5 × 10^-8, corresponding to a difference of about 29.2 times. Because both peaks are concentrated within the same narrow spectral window near 794.7 nm, it is clear that the nonlinear enhancement does not simply originate from an intrinsic material difference, but is resonantly amplified by the qBIC with strong helicity selectivity.

This large contrast arises from the synergistic action of three factors. First, WS_2 itself possesses strong second-order nonlinearity [10-12]. Second, the qBIC provides strong near-field localization at the pump frequency, substantially enhancing the local pump field inside the two-dimensional material [3,4]. Third, true chirality makes this field enhancement strongly favorable to only one incident helicity, thereby converting a linear chiral difference into a much larger nonlinear output contrast [8,13]. The nonlinear contrast is therefore not the consequence of a single mechanism, but the product of material nonlinearity, modal enhancement, and chiral selectivity.

The spectral behavior in Figure 5 is equally instructive. Both curves peak within the same narrow spectral window around 794.7 nm, which shows that the enhancement process is explicitly resonance mediated. Away from this wavelength, the nonlinear signal rapidly decreases, indicating that the advantage provided by the qBIC is not a broadband background effect, but a narrowband enhancement tightly bound to the linewidth of a high-Q resonance. For polarization-selective frequency-conversion devices, this combination of narrow bandwidth and high contrast is precisely what makes the platform attractive.

It should also be noted that the dominant linear channel in Figure 2 does not have to coincide exactly with the dominant nonlinear channel in Figure 5. Maximum far-field transmission, maximum internal energy storage, and maximum nonlinear overlap are not identical optimization targets. Practical design therefore requires the simultaneous consideration of resonant coupling, local field distribution, and the position of the active material, rather than judging the nonlinear performance solely from the far-field transmission peak. The present dataset is compelling precisely because it displays a clear internal correspondence among the far-field spectra, the near-field distributions, and the nonlinear conversion efficiency.

6. Summary

A global analysis of the supplied data confirms that this hybrid G-shaped $TiO_2/SiO_2/WS_2$ metasurface constitutes a truly chiral nonlinear nanophotonic platform governed by qBIC physics. The 10° perturbation opens a high-Q mode that would otherwise remain symmetry protected, the G-shaped geometry and vertically asymmetric layering jointly endow the device with strong circular-polarization selectivity, and WS_2 serves as an efficient second-order nonlinear source. As a result, the device simultaneously realizes narrowband linear chiral response, helicity-dependent near-field hotspots, and high-contrast nonlinear conversion in the vicinity of 794.7 nm.

The core mechanism lies in the synergy between qBIC-enhanced local fields and the large second-order nonlinearity of WS_2. The qBIC increases the local field intensity and compresses the spectral window, true chirality determines that this enhancement preferentially acts on only one circularly polarized helicity, and WS_2 converts this linear field imbalance into a pronounced nonlinear output contrast. This device therefore provides a clear and convincing design paradigm for ultracompact, highly selective, and strongly field-enhanced chiral nonlinear metasurfaces.

Acknowledgments

National Natural Science Foundation of China (Grant No.11604057).

References

[1] C. W. Hsu, B. Zhen, A. D. Stone, J. D. Joannopoulos, and M. Soljačić. Bound states in the continuum. *Nature Reviews Materials* 2016, **1**, 16048.

[2] K. Koshelev, S. Lepeshov, M. Liu, A. Bogdanov, and Y. Kivshar. Asymmetric metasurfaces with high-Q resonances governed by bound states in the continuum. *Physical Review Letters* 2018, **121**(19), 193903.

[3] L. Carletti, K. Koshelev, C. De Angelis, and Y. Kivshar. Giant nonlinear response at the nanoscale driven by bound states in the continuum. *Physical Review Letters* 2018, **121**(3), 033903.

[4] M.-S. Hwang, K.-Y. Jeong, J.-P. So, K.-H. Kim, and H.-G. Park. Nanophotonic nonlinear and laser devices exploiting bound states in the continuum. *Communications Physics* 2022, **5**(1), 106.

[5] Y. Tang and A. E. Cohen. Optical chirality and its interaction with matter. *Physical Review Letters* 2010, **104**(16), 163901.

[6] H. S. Khaliq, A. Nauman, J.-W. Lee, and H.-R. Kim. Recent progress on plasmonic and dielectric chiral metasurfaces: fundamentals, design strategies, and implementation. *Advanced Optical Materials* 2023, **11**, 2300644.

[7] L. Kühner, F. J. Wendisch, A. A. Antonov, J. Bürger, L. Hüttenhofer, L. de S. Menezes, S. A. Maier, M. V. Gorkunov, Y. Kivshar, and A. Tittl. Unlocking the out-of-plane dimension for photonic bound states in the continuum to achieve maximum optical chirality. *Light: Science & Applications* 2023, **12**, 250.

[8] K. Koshelev, Y. Tang, Z. Hu, I. I. Kravchenko, G. Li, and Y. Kivshar. Resonant chiral effects in nonlinear dielectric metasurfaces. *ACS Photonics* 2023, **10**(1), 298-306.

[9] N. Kumar, S. Najmaei, Q. Cui, F. Ceballos, P. M. Ajayan, J. Lou, and H. Zhao. Second harmonic microscopy of monolayer MoS2. *Physical Review B* 2013, **87**(16), 161403(R).

[10] C. Janisch, Y. Wang, D. Ma, N. Mehta, A. L. Elías, N. Perea-López, M. Terrones, V. Crespi, and Z. Liu. Extraordinary second harmonic generation in tungsten disulfide monolayers. *Scientific Reports* 2014, **4**, 5530.

[11] G. T. Forcherio, J. Riporto, J. R. Dunklin, Y. Mugnier, R. Le Dantec, L. Bonacina, and D. K. Roper. Nonlinear optical susceptibility of two-dimensional WS2 measured by hyper-Rayleigh scattering. *Optics Letters* 2017, **42**(23), 5018-5021.

[12] K. Bredillet, J. Riporto, G. T. Forcherio, J. R. Dunklin, J.-P. Wolf, L. Bonacina, Y. Mugnier, and R. Le Dantec. Dispersion of the nonlinear susceptibility of MoS2 and WS2 from second-harmonic scattering spectroscopy. *Physical Review B* 2020, **102**(23), 235408.

[13] N. Bernhardt, K. Koshelev, S. J. U. White, K. W. C. Meng, J. E. Fröch, S. Kim, T. T. Tran, D.-Y. Choi, Y. Kivshar, and A. S. Solntsev. Quasi-BIC resonant enhancement of second-harmonic generation in WS2 monolayers. *Nano Letters* 2020, **20**(7), 5309-5314.

[14] V. Kravtsov, E. Khestanova, F. A. Benimetskiy, T. S. Ivanova, A. P. Samusev, I. S. Sinev, D. G. Pidgayko, A. S. Mozharov, I.

S. Mukhin, M. S. Lozhkin, Y. V. Kapitonov, A. S. Brichkin, M. V. Petrov, V. S. Volkov, D. N. Krizhanovskii, I. V. Iorsh, and A. N. Grigorenko. Nonlinear polaritons in a monolayer semiconductor coupled to optical bound states in the continuum. *Light: Science & Applications* 2020, **9**, 56.

[15] E. Maggiolini, L. Polimeno, F. Todisco, A. Di Renzo, B. Han, M. De Giorgi, V. Ardizzone, C. Schneider, R. Mastria, A. Cannavale, M. Pugliese, L. De Marco, A. Rizzo, V. Maiorano, G. Gigli, D. Gerace, D. Sanvitto, and D. Ballarini. Strongly enhanced light-matter coupling of monolayer WS2 from a bound state in the continuum. *Nature Materials* 2023, **22**(8), 964-969.